Model of Soft-Switching Converter and Power Control for Smart Grid Applications

Roberto Zanasi and Stefania Cuoghi

Abstract—**The advances in computing and communication technologies allow to connect inverters of energy generation systems in smart grids, to well control the power flows. Modeling tools would be helpful in the design of required new inverter topology. This paper presents a modeling technique, so called Power Oriented Graph, easy to use and to be implemented in Matlab-Simulink environment. This technique has been used for modeling a recently proposed soft-switching grid-connected DC/AC power converter for photovoltaic systems. Modifications in the structure of the DC/DC converter and in the control of the DC/AC converter for smart grid applications are proposed. Simulation results confirm the effectiveness of the presented models and the introduced improvements.**

Index Terms—**Modeling technique, DC/DC converter, DC/AC converter, power control.**

I. Introduction

Nowadays the growth in peak demand for electricity and the increasing of distributed and deregulated energy systems require an optimized grid control. The advances in computing and communication technologies [1] allow to transform the traditional power network into a smart grid, capable of real-time remote monitoring and control. Smart grids are particularly well-suited for renewable energy sources, whose power flow is intermittent, depending upon the availability of natural resources.

In the architecture of smart grids the inverters play an active role, communicating data in real-time and receiving control parameters by the remote control, on the base of energy managements strategies [2]. The main goals of these strategies are the reduction of load peaks generated by consumers during the day, the reliability and the affordability of the grid. Moreover, the utility grid has to supply reactive power to compensate the effects of industrial inductive loads, such as induction motors. It is well known that reactive power flow wastes energy and transmission capacity, causing voltage droop and possible blackouts [3]. In a smart grid architecture the inverters can manage the reactive power flow locally at distribution level, on the base of Boucherot theorem. In this scenario modeling tools would be helpful to manufacturers to analyze and design new topologies of inverters, improving their cost and efficiency [4]-[6], and to implement new active controls based on data transmissions. Commercial tools need to be continuously updated, since often have not all the necessary components to simulate the converters or can not operate with high switching frequency. In this paper an accurate model of a photovoltaic (PV) inverter architecture recently proposed in [7] is presented. The model has been obtained using the Power Oriented Graph (POG) technique, which can be easily implemented and simulated in Matlab-Simulink environment [8]-[10]. The analyzed and simulated system is based on a single-phase soft-switching 3kW DC/AC power inverter. Three variants of the DC/DC converter with and without transformer are modeled using POG technique, showing how this can be easily done.

The paper is organized as follows. In section II the Power Oriented Graphs modeling technique is presented. In section III the considered grid-connected PV system is described and modeled. Thee variants on the DC/DC converter with and without transformer are presented. A control algorithm for regulating the power factor in a smart-grid structure is proposed. Simulations of the proposed power conversion system and conclusions end the paper.

R. Zanasi and S. Cuoghi are with the Faculty of Engineering, DII-Information Engineering Department, University of Modena and Reggio Emilia Via Vignolese 905, 41100, Modena, Italy, e-mails: roberto.zanasi@unimore.it and stefania.cuoghi@unimore.it.

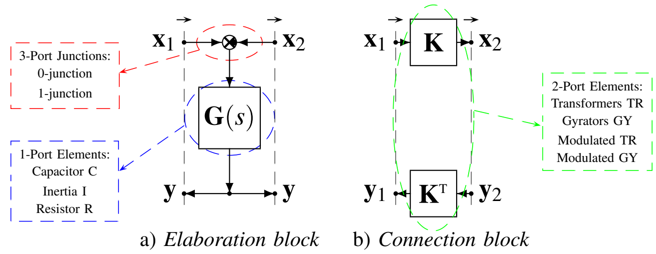

Fig. 1. POG basic blocks: *elaboration block* and *connection block*.

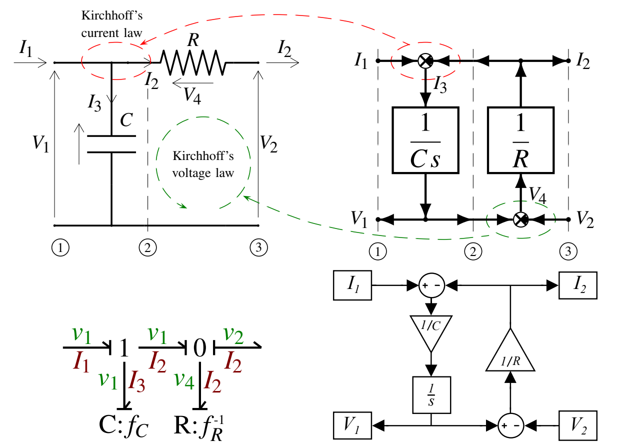

Fig. 2. Electrical circuit of CR filter, corresponding POG model, BG model and Matlab/Simulink scheme.

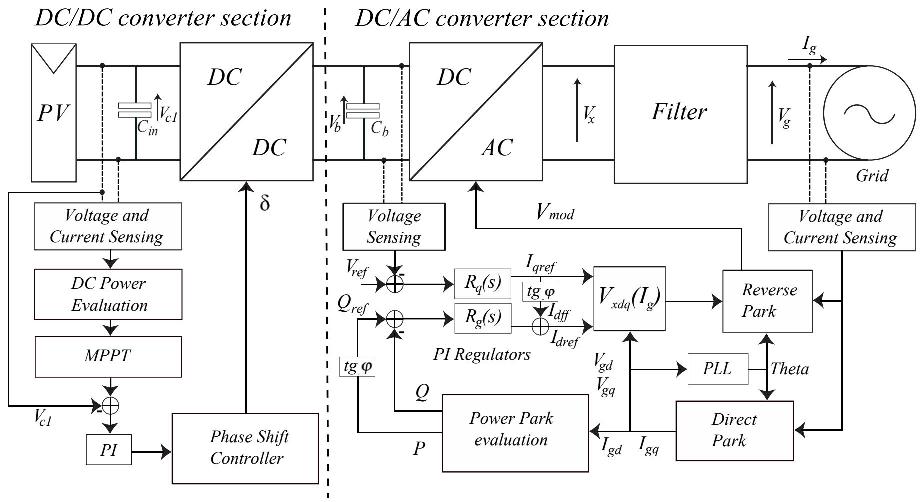

Fig. 3. Blocks scheme of the considered grid-connected PV system.

II. The Power-Oriented Graphs (POG) technique

The POG is a graphical modeling technique based on the same energetic approach of the Bound Graph (BG) technique, but it uses a different graphical notation. The two POG basic blocks are the elaboration block and the connection block, see Fig. 1. The first is used for modeling all the physical elements that can store and/or dissipate energy, while the second is used for modeling all the physical elements that transform the power without losses. The elaboration block corresponds to the 1-port element in BG technique (capacitor, inertia, resistor), while the sum block at the top of the elaboration block corresponds to the 3-port BG connection elements (0-junctions or 1-junctions). The connection block denotes all the 2-port elements of the BG technique: transformer, gyrators, modulated transformer and modulated gyrators. The dashed lines in Fig. 1 denote the power sections which connect the POG blocks to the external world. The scalar product $\mathbf{x}^{\mathrm{T}}\mathbf{y}$ of the two *power vectors* $\mathbf{x}$ and $\mathbf{y}$ involved in each dashed line of a POG schema, have the physical meaning of *the power flowing through that particular section*, see Fig. 1.

Let us consider the simple electrical example of the CR filter shown in Fig. 2. The corresponding POG model is shown on the top right, while the BG model is shown on the bottom left of the figure. Both the techniques provide the exact mathematical model of the system. While the BG scheme is quite compact, the POG model is easy to use, easy to understand and can be directly implemented in Matlab-Simulink environment, see the block scheme on the bottom right of Fig. 2.

III. System structure

Let us consider the block scheme of the grid-connected PV system shown in Fig. 3, which is an improved version of the power converter proposed in [7]. The upper part represents the hardware section, which includes a dual active-bridge DC/DC converter, a single-phase buck 3kW DC/AC converter and a low-pass filter. The control of the power flow towards the grid is obtained in practical implementation by using a microcontroller and is based on the control of active and reactive power flows. In particular, the DC/DC converter is controlled by a Maximum Power Point Tracking (MPPT) algorithm to extract the maximum possible power from the PV panels. The control of the DC/AC converter synchronizes the output voltage of the converter with the grid voltage $V_g(t)$ using a Phase Locked Loop (PLL) algorithm. The output active and reactive power flows are regulated in order to maintain the bus voltage V_b to a constant value V_{ref} and to satisfy the power factor required by the smart grid control.

IV. Power-Oriented Graphs dynamic model of the hardware structure

The electrical scheme of the hardware structure and the corresponding POG model are shown in Fig. 4 and 7 respectively. The dashed lines ①:⑧ in Fig. 7 are in direct correspondence with the physical power sections ①:⑧ of the POG model.

A. The DC/DC converter section (sec.1:5)

It can be easily shown that the POG model of the input filter $R_{in}C_{in}$ is the block schema shown in sec. ①-② of Fig. 7. Sec. ②:⑤ denote the model of the DC/DC converter, which is designed to boost the voltage of the PV panels from a minimum input of 150V to a DC value regulated at $V_{ref} = 450$V. The transformer is modeled on the base of the following classical equations, which describe the dynamic behavior of primary and secondary currents I_p, I_s and voltages V_p, V_s in ideal conditions

$$L_p\dot{I}_p + M\dot{I}_s = V_p - R_pI_p, \qquad L_s\dot{I}_s + M\dot{I}_p = V_s - R_sI_s, \quad (1)$$

where L_p, L_s and M are the self and mutual inductances of the transformer, R_p and R_s are the corresponding transformer resistances. Relations (1) can be expressed in the matrix form as follows

$$\underbrace{\begin{bmatrix} L_p & M \\ M & L_s \end{bmatrix}}_{\mathbf{L}_T}\underbrace{\begin{bmatrix} \dot{I}_p \\ \dot{I}_s \end{bmatrix}}_{\dot{\mathbf{I}}_{ps}} = \underbrace{\begin{bmatrix} -R_p & 0 \\ 0 & -R_s \end{bmatrix}}_{-\mathbf{R}_T}\underbrace{\begin{bmatrix} I_p \\ I_s \end{bmatrix}}_{\mathbf{I}_{ps}} + \underbrace{\begin{bmatrix} V_p \\ V_s \end{bmatrix}}_{\mathbf{V}_{ps}}. \quad (2)$$

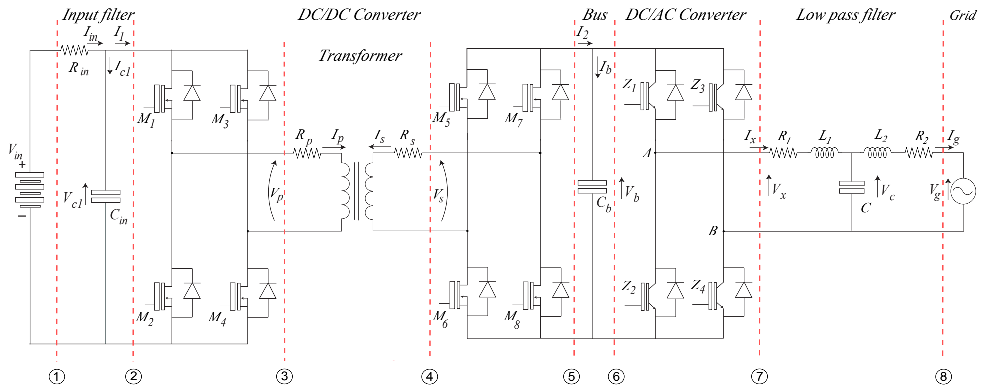

Fig. 4. Complete hardware structure of the PV system connected to the grid.

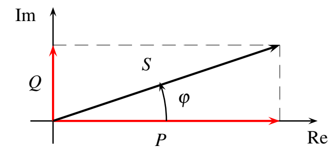

Fig. 5. Active and reactive power P/Q relationship.

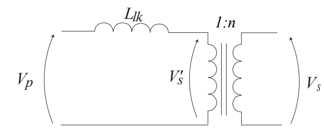

Fig. 6. Primary-referred equivalent circuit of the transformer.

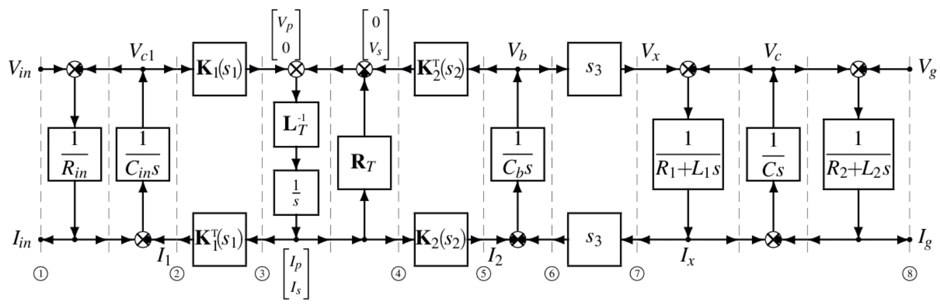

Fig. 7. POG dynamic model of the PV system described in Fig. 4.

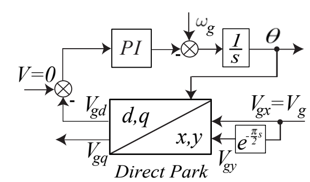

Fig. 8. PLL algorithm

From (2) one obtains that the POG model of the transformer is characterized by the matrices $\mathbf{L}_T$ e $\mathbf{R}_T$, as shown in sec. ③-④.

The dynamic models of the input and output bridges are described by the connection blocks shown in sec. ②-③ and ④-⑤, and is obtained on the base of the operating principle of the converter, described in [7] and [11]. The control is based on the zero-voltage-switching (ZVS) PWM technique and operates in a soft-switched manner [12], [14], [13]. The waveforms of the main signals of the converter are shown in red in Fig. 9, where $\theta = \omega t$, $\omega = 2\pi f_s$ and f_s is the switching frequency. Variable $M_i(\theta)$ denotes the control input of the i-th MOS: when $M_i = 1$ the MOS is ON, when $M_i = 0$ the MOS is OFF. In particular, the converter is controlled by regulating the phase-shift δ between signal $M_5(\theta) = \overline{M}_6(\theta)$ of the active bridge and signal $M_1(\theta) = M_4(\theta)$ of the input bridge. The value of δ is determined by the Maximum Power Point Tracking (MPPT) algorithm, which implements a classical version of perturb and observed method [7], [15]. The transformer secondary current I_s has the same behavior of primary current I_p with the opposite sign. The control signals $s_1(t)$ and $s_2(t)$ in the matrices $\mathbf{K}_1(s_1)$ and $\mathbf{K}_2(s_2)$ of the POG model of Fig. 7 are obtained by imposing the conservation of the input-output power and neglecting the dissipative losses of the MOS. From the waveforms of signals in Fig. 9, one obtains the following relation

$$s_1(t) = \frac{V_p(t)}{V_{c1}(t)} = \frac{I_1(t)}{I_p(t)} = 2\big(M_1(t) \oplus \overline{M}_3(t)\mathrm{sgn}\bar{I}_p(t) - 0.5\big), \quad (3)$$

where $V_{c1}(t)$ and $I_1(t)$ are respectively the converter input voltage and current. Signal $s_1(\theta)$ has the same waveform of $V_p(\theta)$ in Fig. 9 normalized to values $\{1, -1\}$. The control signal $s_2(t) = \frac{V_s(t)}{V_b(t)} = \frac{I_2(t)}{I_s(t)}$ can be expressed as follows:

$$s_2(t) = 2\left[M_1\left(t+\frac{\delta}{\omega}\right) \oplus \overline{M}_3\left(t+\frac{\delta}{\omega}\right)\mathrm{sgn}\bar{I}_s(t) - 0.5\right].$$

1) Variants on the DC/CD converter: The DC/DC converter topology can be modified considering an output half-bridge instead of an output full-bride, see Fig. 10. The corresponding waveforms of the main signals are shown by the blue dashed lines in Fig. 9. This solution has the advantage of decreasing the number of devices and the cost of the converter. The corresponding POG model is shown on the right side of Fig. 10. The mathematical relation of control signal s_1 in the connections blocks of the input bridge is still given by (3), while the control $s_2'(t)$ of the output half-bridge can be expressed as follows

$$s_2'(t) = \frac{V_s(t)}{V_b(t)} = \frac{I_2(t)}{I_s(t)} = \big(M_5(t)\bar{I}_s(t) - \overline{M}_5(t)I_s(t)\big).$$

Referring to the equivalent circuit shown in Fig. 6, the transformer leakage inductance L_{lk} is used as energy storing and transferring element during the circuit operation [13]. If the transformer is substituted by an inductance as shown in Fig. 11 and 12, the converter still operates as described in the previous topologies. The modified topologies can be considered as particular cases of the converters with transformer when $L_{lk} = L$ or $L_{lk} = L'$ and $n = 1$. The waveforms of the main signals are still shown in Fig. 9, where $V_p = V_{L1} = V'_{L1}$, $V_s = V_{L2}$ and $I_p = I_L$ in the case of output full-bridge (red lines) and $V_s = V'_{L2}$ and $I_p = I'_L$ in the case of output half-bridge (dashed blue line). The corresponding POG models in transformerless cases have a scalar structure, see Fig. 11- 12. The control signal s_1 is still given by (3), while the control signals $s_{2L}(t) = \frac{V_{12}(t)}{V_b(t)} = \frac{-I_2(t)}{I_L(t)}$ and $s'_{2L} = \frac{V'_{12}}{V_b(t)} = \frac{-I_2(t)}{I'_L(t)}$ of the output full-bridge and half-bridge can be expressed as follows

$$s_{2L}(t) = 2\left(M_1\left(t+\frac{\delta}{\omega}\right) \oplus \overline{M}_3\left(t+\frac{\delta}{\omega}\right)\mathrm{sgn}I_L(t) - 0.5\right),$$

$$s'_{2L}(t) = \left(M_5(t)I'_L(t) - \overline{M}_5(t)\overline{I}'_L(t)\right).$$

2) Mathematical expression for the power flow: From the converter operation modes previously described and from the idealized waveforms in steady-state conditions shown in Fig. 9, it follows that the power P_{av} transferred to the output in a half switching period in the case of full-bridge DC/DC converter with transformer can be expressed as follows [7]

$$P_{av} = \frac{V_{c1}^2}{\omega L_{lk}}\delta d\left(1-\frac{\delta}{\pi}\right), \tag{4}$$

where $d = \frac{V_b}{nV_{c1}}$. Expression (4) can also be used in the case of full-bridge transformerless DC/DC converter when $n = 1$ and $L_{lk} = L$. In the case of half-bridge DC/DC converter with transformer, the power P'_{av} transferred to the output in a half switching period can be expressed as follows

$$\begin{aligned} P_{av'} = \; & \frac{V_{c1}^2 \pi d}{2\omega L_{lk}(2+d)^2}\left[1+d-2d^2+\right. \\ & \left. +\left(\frac{\delta}{\pi}\right)4(d^2+d+1) - \left(\frac{\delta}{\pi}\right)^2 2(d^2+2d+2)\right]. \end{aligned} \tag{5}$$

Expression (5) can be also used in the case of full-bridge transformerless DC/DC converter when $n = 1$ and $L_{lk} = L'$. Given the values of parameters V_b, n and L_{lk} (or L and L'), relations (4) and (5) show how the output power can be regulated choosing the values of V_{c1} and δ.

B. The DC/AC converter section (sec. 5:8)

It can be easily shown that the POG model of the bus capacitor C_b is described by the sec. ⑤-⑥ in Fig. 7. The model of the IGBT full-bridge DC/AC converter is described by connection block shown in sec. ⑥-⑦, where s_3 is the unipolar PWM control signal. This signal is determined comparing the PWM triangular carrier $V_t(t)$ with the modulation voltage $V_{mod}(t)$ normalized with respect to the bus voltage $V_b(t)$ as follows:

$$s_3(t) = \frac{\mathrm{sgn}\left(V_t(t) + \frac{V_{mod}(t)}{V_b(t)}\right) - \mathrm{sgn}\left(V_t(t) - \frac{V_{mod}(t)}{V_b(t)}\right)}{2}. \tag{6}$$

Using (6) the modulated voltage $V_x(t) = s_3(t)V_b(t)$ switches between the three levels $\{+V_b, -V_b, 0\}$.

The LCL filter has been designed to reduce the high-order harmonics introduced by the PWM modulation, according to the methods described in [16] and [7]. The corresponding POG model is shown in sec. ⑦-⑧ of Fig. 7.

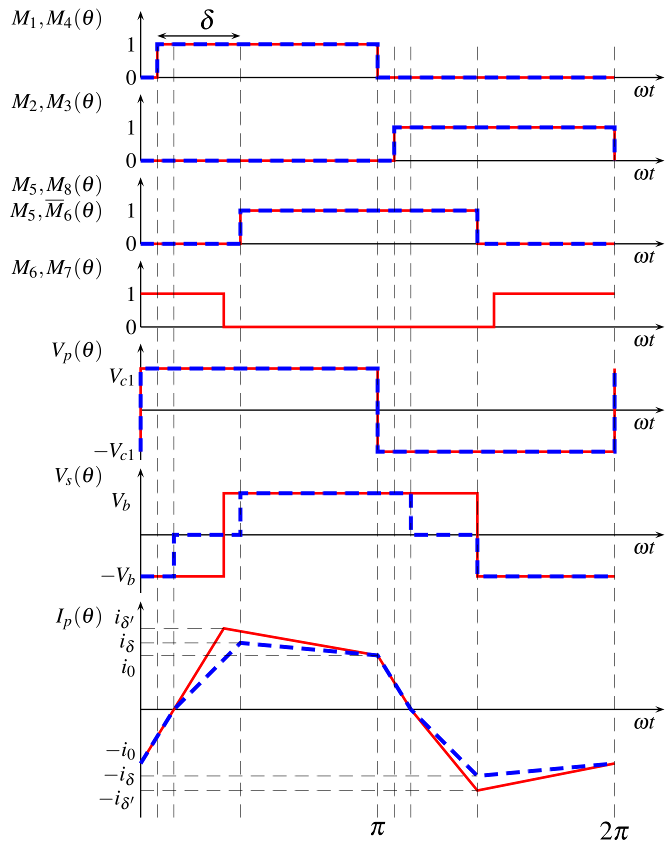

Fig. 9. Idealized voltage and current waveforms of the transformer in the case of output full-bridge (red lines) and half-bridge (dashed blue lines).

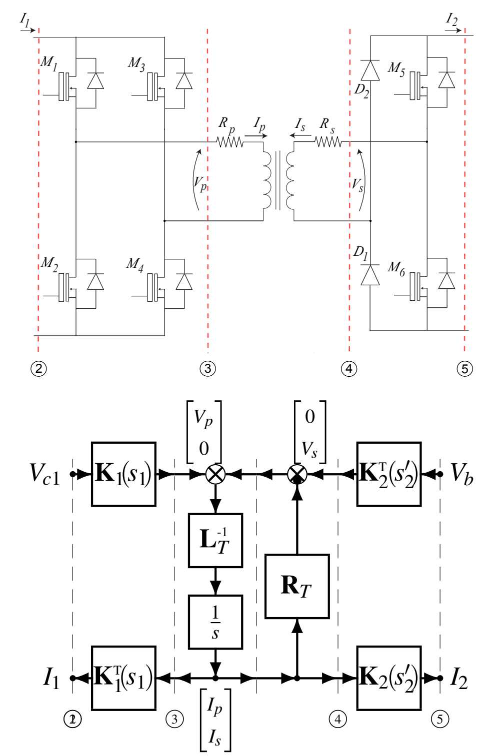

Fig. 10. Electrical scheme and POG model of the DC/DC converter with output half-bridge and transformer.

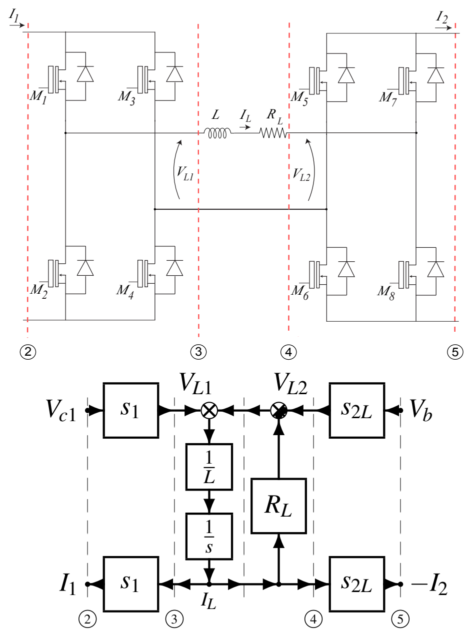

Fig. 11. Electrical scheme and POG model of the transformerless DC/DC converter with output full-bridge .

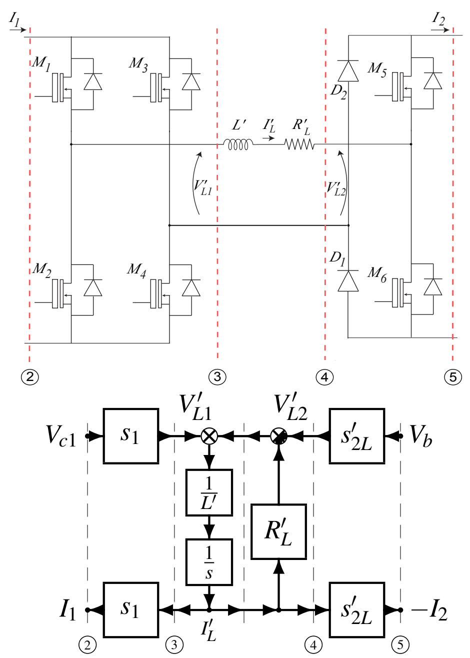

Fig. 12. Electrical scheme and POG model of the transformerless DC/DC converter with output half-bridge.

It is easy to see that the state space equations of the POG model of Fig. 7 can be expressed in the form $\mathbf{L}\dot{\mathbf{x}} = -\mathbf{A}\,\mathbf{x} + \mathbf{B}\,\mathbf{u}$, where:

$$\mathbf{L} = \begin{bmatrix} C_{in} & 0 & 0 & 0 & 0 & 0 \\ 0 & \mathbf{L}_T & 0 & 0 & 0 & 0 \\ 0 & 0 & C_b & 0 & 0 & 0 \\ 0 & 0 & 0 & L_1 & 0 & 0 \\ 0 & 0 & 0 & 0 & C & 0 \\ 0 & 0 & 0 & 0 & 0 & L_2 \end{bmatrix}, \quad \mathbf{x} = \begin{bmatrix} V_{c1} \\ \mathbf{I}_{ps} \\ V_b \\ I_x \\ V_c \\ I_g \end{bmatrix}, \quad \mathbf{I}_{ps} = \begin{bmatrix} I_p \\ I_s \end{bmatrix},$$

$$\mathbf{A} = \begin{bmatrix} \frac{1}{R_{in}} & \mathbf{K}_1^{\mathrm{T}} & 0 & 0 & 0 & 0 \\ -\mathbf{K}_1 & \mathbf{R}_T & -\mathbf{K}_2^{\mathrm{T}} & 0 & 0 & 0 \\ 0 & \mathbf{K}_2 & 0 & s_3 & 0 & 0 \\ 0 & 0 & -s_3 & R_1 & 1 & 0 \\ 0 & 0 & 0 & -1 & 0 & 1 \\ 0 & 0 & 0 & 0 & -1 & R_2 \end{bmatrix}, \quad \mathbf{B} = \begin{bmatrix} \frac{1}{R_{in}} & 0 \\ 0 & 0 \\ 0 & 0 \\ 0 & 0 \\ 0 & 0 \\ 0 & -1 \end{bmatrix},$$

$$\mathbf{u} = \begin{bmatrix} V_{in} \\ V_g \end{bmatrix}, \; \mathbf{L}_T = \begin{bmatrix} L_p & M \\ M & L_s \end{bmatrix}, \; \mathbf{R}_T = \begin{bmatrix} R_p & 0 \\ 0 & R_s \end{bmatrix}, \; \begin{matrix} \mathbf{K}_1(s_1) = [s_1 \;\, 0]^{\mathrm{T}} \\ \mathbf{K}_2(s_2) = [0 \;\, s_2] \end{matrix}.$$

1) Control algorithm: The digital control of the DC/AC section has to compensate the gain and the phase shift introduced by the LCL filter at grid frequency and to regulate the power flow as required by the smart grid.

The proposed algorithm is based on Park transformations of sensed grid voltage $V_g(t)$ and current $I_g(t)$ and on Akagi's *pq* theory [17]-[21]. In stationary *xy* reference frame, the voltage $V_g(t)$ and the current $I_g(t)$ can be expressed as follows

$$V_g(t) = V\cos(\omega t + \phi_V) + jV\sin(\omega t + \phi_V) = V_{gx}(t) + jV_{gy}(t),$$

$$I_g(t) = I\cos(\omega t + \phi_I) + jI\sin(\omega t + \phi_I) = I_{gx}(t) + jI_{gy}(t).$$

Using the Park transformation, the signals $V_g(t)$ and $I_g(t)$ are converted in constant vectors in the dq frame: $\bar{V}_{gdq}(t) = V_{gd}(t) + jV_{gq}(t)$ and $\bar{I}_{gdq}(t) = I_{gd}(t) + jI_{gq}(t)$. The rotating angle θ used in the Park transformations can be obtained by using the digital Phase-Locked Loop (PLL) algorithm shown in Fig. 8, which dynamically synchronizes the q-axis of the dq frame with the rotating vector $V_g(t)$. Using the space vector representation, the modulation voltage can be expressed as $\overline{V}_{mod} = V_x(s)|_{s=j\omega_g}$. Considering the transfer function of the filter, the modulation voltage $V_x(t)$ can be expressed in the dq frame as follows

$$\begin{aligned} V_{xdq}(t) = \; & \bar{V}_{gqd}(t)(1 - L_1 C\omega_g^2 + jR_1 C\omega_g) + \\ & + \bar{I}_{gref}(t)[R_1 + R_2 - (L_1 R_2 + L_2 R_1)C\omega_g^2 + \\ & + j((R_1 R_2 C + L_1 + L_2)\omega_g - L_1 L_2 C\omega_g^3)]. \end{aligned} \tag{7}$$

Relation (7) is implemented by the block "$V_{xdq}(I_g)$" in Fig. 3. The grid voltage $\bar{V}_{gqd}(t)$ is given by the sensing system, while the desired grid current $\bar{I}_{gref}(t)$ is dynamically calculated by the control system. The desired active grid current $I_{qref}(t)$ is regulated in dq frame by using a PI compensator which acts on the grid current $I_g(t)$ and maintains the bus voltage $V_b(t)$ equal to the reference value V_{ref}. In this way the active power P is controlled to transfer to the grid all the ative power coming from PV panels. The reactive grid current $I_{dref}(t)$ is regulated by a second PI compensator to achieve the power factor $\cos\varphi$ required by the smart grid, where φ is the desired phase angle between the grid current I_g and the grid voltage V_g.

The relationship between the active power and the reactive power is shown in Fig. 5, where the apparent power $S = \sqrt{P^2 + Q^2}$ is the magnitude of the complex power $\overline{S} = P + jQ = Se^{j\varphi}$. In the case of required unity power factor $cos\varphi = \frac{P}{S} = 1$, the reactive power Q is regulated to be zero and $I_g(t)$ is synchronized with $V_g(t)$. In the case $cos\varphi \neq 1$ the reactive power Q is controlled by the reference value $Q_{ref} = P\tan\varphi$, where P is the sensed active power.

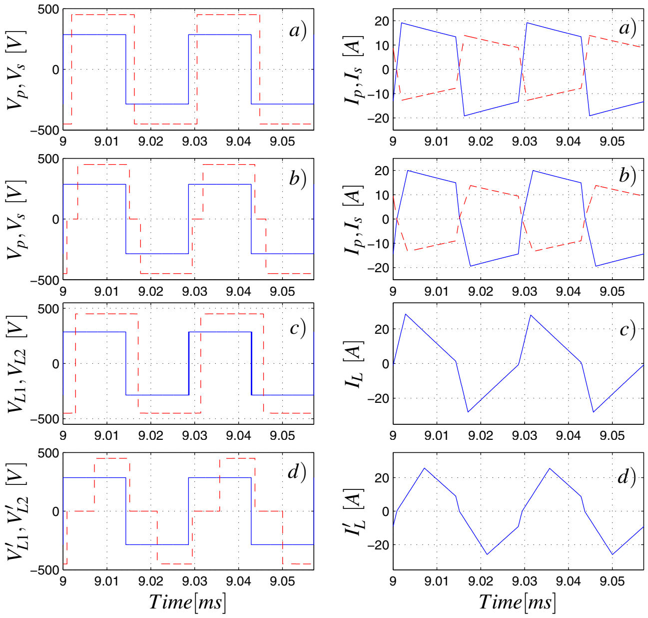

Fig. 13. Input and output currents and voltages of DC/DC converter in steady state in the cases *a*), *b*), *c*) and *d*).

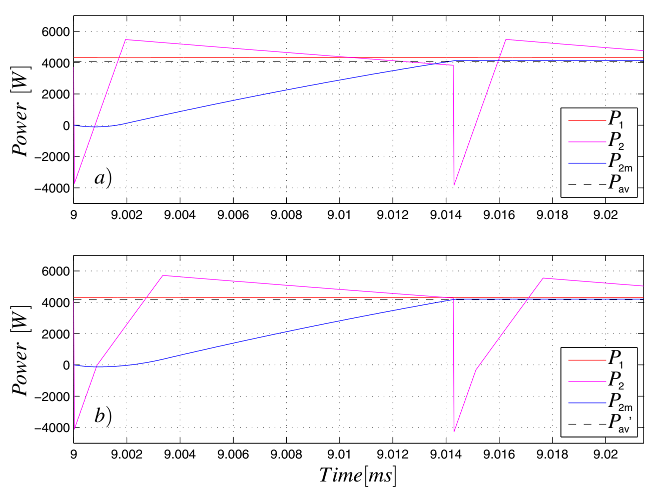

Fig. 14. Powers P_1 and P_2 flowing through sections 1 and 2, total power P_{2m} flowing through section 2 in half switching period and theoretical output power P_{av} P'_{av} calculated using (4) and (5) in cases *a*) and *b*).

V. Simulation results

The presented simulation results have been obtained using the following parameters. DC/DC converter: $V_{in} = 300$ V, $V_b = 450$V, $R_{in} = 1\Omega$, $L_{lk} = 35\mu$H, $n = 1.5$, $L_p = 2.1$mH, $L_s = 4.8$mH, $L = L' = 70\mu$H, $M = 3.2$mH, $R_p = 0.15\Omega$, $R_s = 0.225\Omega$, DC/DC switching frequency $f_s = 35$kHz, $S_1 = 0.01\pi$. The phase shift δ has been set to the following values: *a*) 0.1348π for the output full-bridge with transformer, *b*) 0.2345π for the output half-bridge with transformer, *c*) 0.196π for the output full-bridge without transformer and *d*) 0.5π for the output half-bridge without transformer.

DC/AC converter: PWM carrier frequency $f_c = 17\,kHz$, grid frequency $f_g = 50\,Hz$, $C = 5\,\mu F$, $L_1 = 1.8\,mH$, $L_2 = 0.9\,mH$, $R_1 = 0.1\,\Omega$, $R_2 = 0.05\,\Omega$ and $V_{ref} = 450$ V. PI controller $R_q(s)$ of variable I_{qref}: $R_q(s) = 1.8 + \frac{25}{s}$. PI controller $R_d(s)$ of variable I_{dref}: $R_d(s) = 0.001 + \frac{0.01}{s}$. PI controller $R_L(s)$ in the PLL algorithm: $R_L(s) = 1 + \frac{30}{s}$.

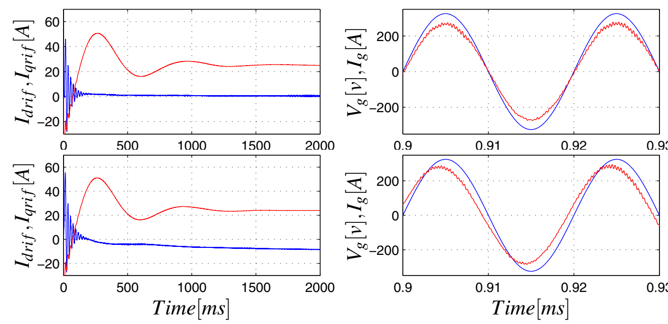

Fig. 15. Reference active and reactive currents I_{qrif}, I_{drif} and zoom of grid current I_g multiplied by 10 and grid voltage V_g when $\varphi = 0$ and $\varphi = 20^o$.

The waveforms of voltages and currents of the DC/DC converter in the considered configurations are shown in Fig. 13, they exactly correspond to the idealized behaviors shown in Fig. 9. In steady state conditions the values of the input and bus voltages are $V_{c1} = 285.66 \pm 0.04$V and $V_b = 449.9 \pm 0.03$V. The instantaneous powers $P_1 = V_{in} I_{in}$ and $P_2 = V_{c1} I_1$ flowing through sections ① and ② in cases *a*) and *b*) are shown in red and magenta in Fig. 14. The blue line denotes the total power $P_{2m} = \frac{V_{c1}}{\pi} \int_0^{\pi} i_p(\theta) d\theta$ flowing through sec ② in a half switching period. Notice that the final value of P_{2m}, that is the mean power flowing through sec. ②, is equal to the theoretical output powers P_{av} and P'_{av} calculated using (4) and (5). Moreover the value of P_{av} is equal to $P_1 - R_{in} I_{in}$, as expected. The step response of reference active and reactive currents I_{qref} and I_{dref} of the DC/AC section when the required φ is 0^o and 20^o are shown in red and blue in Fig. 15. Notice that in the first case $I_{dref} = 0$, while in second case I_{dref} is negative, as expected, since the vector $\bar{I}_{gdq}$ is in the second quadrant of the *qd* frame. The right part of Fig. 15 shows that V_g and I_g are synchronized in steady-state when the required φ is 0^o, while I_g has a time shift in advance of about 0.001s when $\varphi = 20^o$, as expected. The powers P_5, P_6 and P_8 flowing through sections ⑤, ⑥ and ⑧ of the system when $\varphi = 0^o$ and $\varphi = 20^o$ are shown in Fig. 16. The blue lines represent the powers $P_5 = V_b I_2$ flowing through section ⑤, while the black and red lines represent the powers flowing through sections ⑥ and ⑧ of the POG scheme of Fig. 7. The ripple present on the power signals is mainly due to the current ripple and it depends on the *LCL* filter design [7]. The magenta and green lines shown in Fig. 16 represent, respectively, the active power P and the reactive power Q flowing towards the grid in steady-state condition. In particular, the mean value of the reactive power Q is equal to zero when $\varphi = 0^o$ and is equal to $P \tan\varphi$ when $\varphi = 20^o$.

VI. Conclusion

In this paper the Power Oriented Graphs technique has been applied to model a recent and innovative soft-switching converter for grid-connected PV systems. Variants on the DC/DC converter with and without transformer has been presented and simulated. A new control strategy for active and reactive power management for smart grid applications has

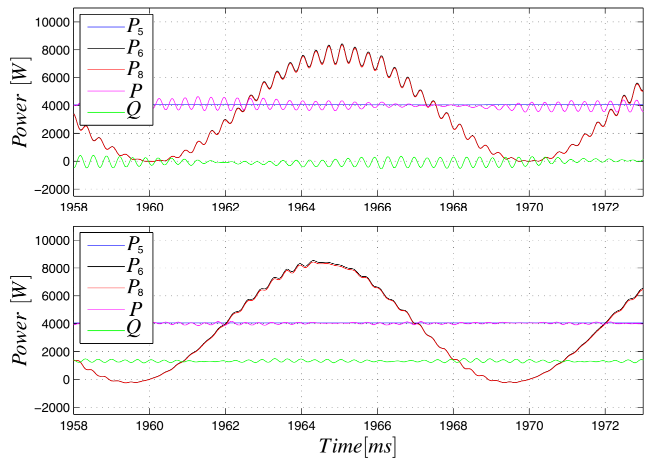

Fig. 16. Power flows P_5, P_6 and P_8 through sections 5, 6 and 8 of the POG scheme when $\varphi = 0^o$ and $\varphi = 20^o$. Active and reactive powers P and Q.

been introduced. The presented simulation results confirm the validity of the POG model and the proposed control strategy. The POG technique would be helpful to manufacturers to analyze and design new inverter topologies, since it is easy to use and it can be directly implemented in Matlab-Simulink environment.

Acknowledgment

The authors would like to thank S. Culzoni, C. Tebaldi and M. Candeli.

References

[1] T. Sauter, M.Lobashov, *End-to-End Communication Architecture for Smart Grids* IEEE Transactions on Industrial Electronics, vol.58, no.4, pp.1218-1228, April 2011

[2] G. Chicco and P. Mancarella , *Distributed multi-generation: A comprehensive view*, Renew. Sustainable Energy Rev., vol. 13, no. 3, pp. 535551, Apr. 2009.

[3] M.S. Kandil, M.M. El-Saadawi, A.E. Hassan, K.M. Abo-Al-Ez, "A proposed reactive power controller for DG grid connected systems,", 2010 IEEE International Energy Conference and Exhibition (EnergyCon) 18-22 Dec. 2010.

[4] W. Li, X. He , *Review of Nonisolated High-Step-Up DC/DC Converters in Photovoltaic Grid-Connected Applications*, IEEE Transactions on Industrial Electronics, vol.58, no.4, pp.1239-1250, April 2011.

[5] EIA, 2011, *Levelized cost of new generation resources in the Annual Energy Outlook* 2011. U.S. Energy Information Administration.

[6] K. Zweibel, *Should solar photovoltaics be deployed sooner because of long operating life at low, predictable cost?* Energy Policy, 38:7519-7530,2010.

[7] M. Cacciato, A. Casoli, R. Attanasio and F. Gennaro *Soft-switching converter with HF transformer for grid-connected photovoltaic systems*, IEEE Transactions on Industrial Electronics, 57(5):1678-86,2010.

[8] R. Zanasi, *Power Oriented Modelling of Dynamical System for Simulation*, IMACS Symp. on Modelling and Control, Lille, France, May 1991.

[9] R. Zanasi, G. H. Geitner, A. Bouscayrol, W. Lhomme, *Different energetic techniques for modelling traction drives*, ELECTRIMACS 2008, Qubec, Canada, June 8-11 2008.

[10] R. Zanasi, *The Power-Oriented Graphs technique: system modeling and basic properties*, Vehicular Power and Propulsion Conference VPPC 2010, Lille, France, 1-3 September 2010.

[11] F. Krismer, S.Round, J.W. Kolar, *Performance Optimization of a High Current Dual Active Bridge with a Wide Operating Voltage Range*, 37th IEEE Power Electronics Specialists Conference PESC '06, 18-22 June 2006.

[12] Y. Jang, M. Jovanovic, Y. Chang, *A new ZVS-PWM full-bridge converter*. IEEE Trans. on Power Electron.: 18(5):1122-1129, Sept. 2003.

[13] H. Li, F. Peng, S. Lawler *A natural ZVS medium-power bidirectional DC-DC converter with minimum number of devices*. IEEE Trans. Ind. Applications, 39(2), 525535, Mar./Apr. 2003.

[14] R.W. De Doncker, D.M. Divan, M.H. Kheraluwala, *A three-phase soft-switched high-power-density DC/DC converter for high-power applications*. IEEE Trans. on Industry Applications: 27(1):63-73, Jan/Feb 1991.

[15] D. Sera, R. Teodorescu, J. Hantschel, and M. Knoll, *Optimized maximum power point tracker for fast-changing environmental conditions*. IEEE Trans. Ind. Electron.: 55(7): 26262637, Jul. 2008.

[16] M. Liserre, R. Teoderuscu, and F. Blaabjerg, *Stability of photovoltaic and wind turbine grid-connected inverters for a large set of grid impedance values*. IEEE Trans. Power Electron.: 21(1), 263272, Jan. 2006.

[17] J.M. Kwon, K.H. Nam and B.H. Kwon. *Photovoltaic power conditioning system with line connection*. IEEE Trans.Ind.Electron.: 53(4):1048-1054, Jun. 2006.

[18] A. Yazdani and R. Iravani, *Voltage-Sourced Converters in Power Systems*. IEEE Pressed 2010.

[19] K. J. strm and B. Wittenmark, *Computer-Controlled Systems Theory and Design*. 3rd ed. Englewood Cliffs, NJ: Prentice-Hall, 1984.

[20] H. Akagi, Y. Kanagawae, and A. Nabae, *Instantaneous reactive power compensator comprising switching devices without energy storage components*. IEEE Trans. Ind. Appl.:IA-20(3), 625634, May/Jun. 1984.

[21] L. G. B. Rolim, D. R. da Costa, and M. Aredes, *Analysis and software implementation of a robust synchronizing PLL circuit based on the pq theory*. IEEE Trans. Ind. Electron.: 53(6), 19191926, Dec. 2006.

Roberto Zanasi received his Laurea degree with honors in Electrical Engineering from the University of Bologna, Italy, in 1986. He received the Ph.D. degree in System Engineering from the University of Bologna in 1992. From 1994 to 1998 he was Researcher in Automatic Control at the Department of Electronics, Computer and System Science, University of Bologna. Since 1998 he has been working at the DII Information Engineering Department at the University of Modena and Reggio Emilia, first as Associate Professor of Automatic Control, and since 2004 as Full Professor. His research interests include: mathematical modelling, Power-Oriented Graphs, simulation, automotive, control of multi-phase electrical motors, variable-structure systems, sliding mode control with integral action, robotics, linear and nonlinear control. He is author or co-author of many technical and scientific publications, and of five books on automatic control, simulation and digital control systems.

Stefania Cuoghi received the Laurea degree in Electronic Engineering in 1999 from the University of Bologna, Italy. Since 2009 she has been working at the University of Modena and Reggio Emilia in Italy, where she is currently working towards the Ph.D degree. Her current research interests include power electronics, power converters, mathematical modelling, Power-Oriented Graphs, simulation, analytical and graphical design of regulators for linear control.